Application of Stereo Imaging to Atomic Force Microscopy

Bernardo D. Aumond, and Kamal Youcef-Toumi

Abstract— Metrological data from sample surfaces can be obtained by using a variety of profilometry methods. Atomic Force Microscopy (AFM), which relies on contact inter-atomic forces to extract topographical images of a sample, is one such method that can be used on a wide range of surface types, with possible nanometer range resolution. However, AFM images are commonly distorted by convolution, which reduces metrological accuracy. This type of distortion is more significant when the sample surface contains high aspect ratio features such as lines, steps or sharp edges - structures commonly found in semiconductor devices and applications. Aiming at mitigating these distortions and recovering metrology soundness, we introduce a novel image deconvolution scheme based on the principle of stereo imaging. Multiple images of a sample, taken at different angles, allow for separation of convolution artifacts from true topographic data. As a result, perfect sample reconstruction and probe shape estimation can be achieved in certain cases. Additionally, shadow zones, which are areas of the sample that cannot be probed by the AFM, are greatly reduced. Most importantly, this technique does not require a priori probe characterization. It also reduces the need for slender or sharper probes, which, on one hand, induce less convolution distortion but, on the other hand, are more prone to wear and damage, thus decreasing overall system reliability.

Keywords— Metrology, Profilometer, Atomic Force Microscope, Deconvolution, Stereo Imaging

I. Introduction

SURFACE characteristics such as topography and critical dimensions, roughness and the area density, shape and location of defects often serve as important indicators of product quality and manufacturing process performance. For such reasons, surface characterization procedures are of primary importance in a wide range of technological fields and across industries. In addition, high precision characterization has played an increasingly important role as the required dimensions of semiconductor and other microfabricated devices continue to shrink into the nanometer and micrometer domains [1].

Various technologies exist that can be used for obtaining high precision images of surfaces. The Atomic Force Microscope (AFM) is one such tool that can be used to profile samples, with possible nanometer level resolution [2]. The AFM generates topographical images via van der Waals forces that arise from direct contact between a sharp probe and a surface. Therefore, this imaging tool can be used to measure several different types of surfaces regardless of other physical attributes such as reflectivity, conductivity or magnetism. It obviously circumvents resolution limitations introduced by diffraction phenomena, associated with optical tools, or by finite electron escape depth, associated with SEM imaging. In addition to that, AFM images consist of three dimensional topographic maps of the surface and are, for this reason, ideal for cross sectional metrology applications. However, despite the AFM's versatility and high resolution, its metrology accuracy is limited by the size and shape of the employed probe [3] due to image convolution.

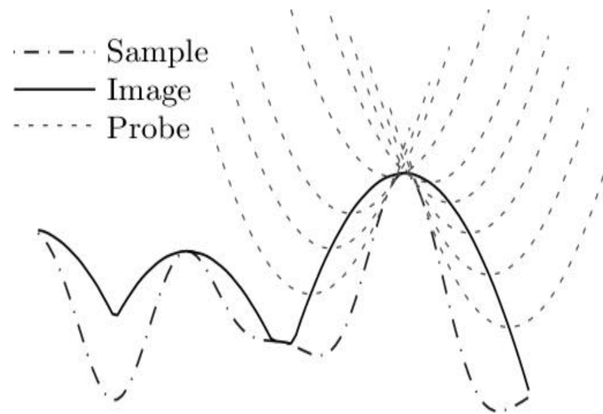

Fig. 1. The probe apex is not necessarily the sole point of contact for high aspect ratio samples. Various positions of the probe along the scan are portrayed.

Image convolution expresses itself in the form of loss of surface detail and dulling of high aspect ratio features. This type of distortion occurs when, during the scanning process, the contact point between the probe and the sample is not the apex of the probe but its side instead, as shown in Figure 1. In other words, during the imaging process, the probe is always externally tangent to the surface, and as a result, the image is a dilated version of the underlying sample. Dilation distortions introduce errors in the metrology data obtained from the surface [4]. As a result, critical dimensions such as linewidth of steps or radius of curvature of high aspect ratio structures (such as field emission probes and high precision cutting edges) become inaccurate [5].

For the sake of semantic accuracy, it should be noted that the term convolution does not strictly apply to the mechanism of image formation in AFM. It has been commonly employed even though no convolution occurs during imaging; dilation instead, is the correct interaction model.

In order to circumvent these limitations, deconvolution algorithms must be developed. These restoration procedures should eliminate metrology distortions in the nanometer level and should also be compatible with high volume inspection tasks. Proposed methodologies must be robust, reliable and easy to implement with commercially available AFM units.

In section II, we introduce the mechanisms of image formation and how they give rise to convolution. In section III, we briefly explain state of the art techniques that can be used for image restoration. In section IV, we introduce a novel stereo imaging procedure that can be used for restoring sample topographies and that can also be used for probe shape estimation and finally in section V, we show introductory results that illustrate the capabilities and versatility of this new technique.

II. IMAGE CONVOLUTION

There exist two widely accepted mechanisms of image formation for AFM. One mechanism model is based on the concept of Legendre Transforms [6], [7] and relies on the assumption that at contact points during scan, the probe and the sample surface share the same gradient or tangent.

In Figure 2, let $S(m)$ be the intercept of the tangent line through the true contact point with the vertical image axis; at that contact point the sample slope is denoted by m and $S(m)$ is denoted the "Legendre Transform of the probe shape at the derivative m". Let $I(m)$ be the intercept of the parallel line through the image point (probe apex) with the vertical image axis. It has been shown elsewhere [7] that the image will also have derivative m at that point. Finally, let $P(m)$ be the intercept of the tangent line through the true contact point with the probe vertical axis. The following relationship holds:

$$S(m) = I(m) + P(m) \quad (1)$$

Given a surface description $y = y(x)$, its Legendre Transform at any derivative $m = \frac{dy}{dx}$ is given by:

$$Y(m) = y(x(m)) - m.x \quad (2)$$

Conversely, if the Legendre Transform of a curve is known, its Cartesian description can be obtained by applying the following inverse transform:

$$\begin{aligned} x &= -\frac{d[Y(m)]}{dm} \\ y &= Y(m) - m\left(\frac{d[Y(m)]}{dm}\right) \\ y &= y(x) \end{aligned} \quad (3)$$

Therefore, if the shape of the probe and the shape of the sample are known, their Legendre Transforms can be obtained according to Equation (2). Then, the Legendre Transform of the resulting image can be computed according to Equation (1). And finally, the shape of the resulting image can be calculated using Equation set (3). However, even though the linear relationship expressed in Equation (1) is simple and straightforward, some implicit assumptions exist. Firstly, the sample and probe geometries must be continuous and, secondly, the sample and probe geometries must not have repeated slopes, that is, they must be convex. This reduces the applicability of this mechanism of image formation to simpler and well defined problems where the implicit assumptions hold [5], [7].

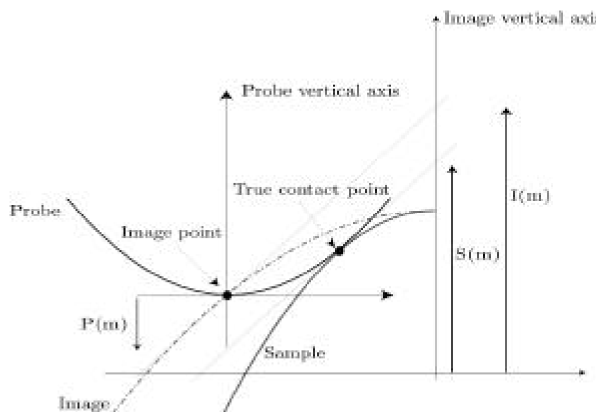

Fig. 2. Mechanism of image formation based on the Legendre Transform model.

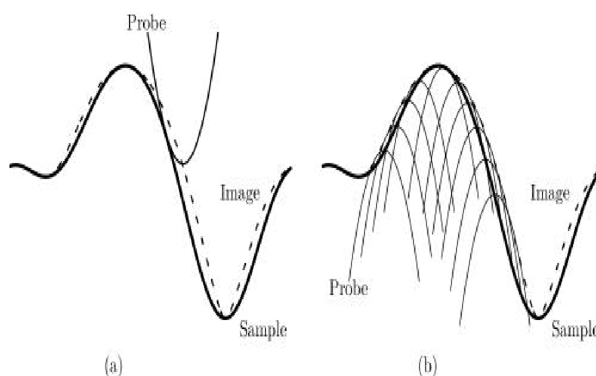

Fig. 3. Mechanism of image formation based on the dilation model. (a) The probe is externally tangent to the sample during the scanning generating the image. (b) A dual and equivalent interpretation is that the image is the combined volume of the translates of the (reflected) probe.

A second mechanism of image formation that is general and makes no geometric assumptions is based on the concept of morphological dilation [4], [8], [9], [10]. The image of a sample is a dilated version of the sample and the structuring element is considered to be the reflected probe shape. That is:

$$I = S \oplus \check{P} \quad (4)$$

where $\check{P}$ is the reflected version of the probe shape P, and S is the sample shape and I, the resulting image.

In other words, if one places a copy of the reflected probe on every single point of the sample surface, with the reflected probe apex coinciding with that surface point, then the surface of the resulting combined volume of all translates of these reflected probes will constitute the image of the sample taken with that specific probe (Figure 3).

A quick analysis of Equation (4) (and of Equation (1) as well) reveals some straightforward conclusions that can be summarized in the following cases:

- Case 1: If the shape of the probe is exactly known and the image is also known, then by applying a reverse mechanism of image formation, the sample shape could be computed, and convolution distortions eliminated.
- Case 2: Conversely, if the sample shape is exactly known and the image is also known, then by applying a reverse mechanism of image

formation, the probe shape could be computed.

- Case 3: If the probe is very sharp compared to the sample dimensions, then the image shape will be very similar to the sample shape, the probe contribution being negligible to image formation.
- Case 4: Conversely, if the sample is very sharp compared to the probe dimensions, then the image shape will be very similar to the reflected probe shape, the sample contribution being negligible to image formation.

These conclusions are the motivation behind current deconvolution or convolution minimization strategies as we discuss is section III.

III. STATE OF THE ART IN IMAGE DECONVOLUTION

In order to recover metrology accuracy, convolution distortions must be eliminated from AFM images. Current deconvolution strategies are based on the realization that Equation (4) (or Equation (1)) establish a system with two unknowns, the probe and the sample geometries (or their Legendre transforms), and one known, the image geometry (or its Legendre transform). In order to solve such an under constrained system, one variable must be determined; that can be accomplished by probe characterization. Another approach is to make the probe so sharp that its contribution to image formation becomes negligible. That would be equivalent to making P in Equation (4) or P(m) in Equation (1) vanish. That is, the system collapses into one known and one unknown and can be solved. The most popular approach though, called blind deconvolution, establishes an estimate for the probe shape, and as a result, a sample estimate can be also obtained.

A. High Aspect Ratio Probes

Convolution distortions are proportional to the probe size relative to the sample size. Therefore, sharp and small probes can be used to minimize convolution distortions, according to Case 3 in section II.

Sharp probes can be obtained by FIB milling conventional AFM probes. Sharpened probes exist in the market with typical radius of curvature of 5 to 20nm. However, for statistical reasons or quality assurance considerations, high volume inspection has become a requirement in many applications. Therefore, long lasting probes must be employed in order to minimize probe replacement due to wear or failure. Sharpened and slender probes are more prone to failure than their larger counterparts and therefore reduce the overall reliability and speed of the inspection system.

Recently, carbon nanotubes have been employed in AFM imaging. Nanotubes are used as probes due to their sharp geometry and mechanical resilience. The carbon nanotubes consist of perfect and seamless graphite shells with dimensions of typically 1nm in diameter and several microns in length. The slenderness of these nanotubes may allow for imaging of high aspect ratio surface features with very small convolution distortions. However, fabrication techniques have yet to be refined [11] and, additionally, lateral flexing of the tube is still a problem when imaging tall structures. As a result of these limitations, imaging with ultra high aspect ratio probes has been mostly confined to off line inspection tasks where scan speeds are slower in order to avoid tip crashes, flexion or excessive wear. Usually, intermittent contact scanning is used in these cases.

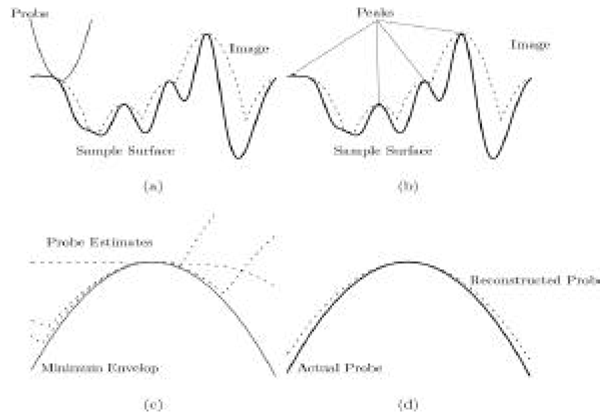

Fig. 4. Blind probe reconstruction. (a) Original Scan. (b) Peaks in image are flagged. (c) Probe estimates are obtained from the individual peaks and the minimum envelop taken as the final probe estimate. (d) Comparison between actual and reconstructed probe.

B. Probe Characterization

Deconvolution can also be accomplished by establishing the shape of the probe and then solving the inverse problem established by Equation (4) or by Equation (1), depending on which mechanism of image formation is used to formulate the problem. According to Case 2 in section II, one could use a sample of known shape, that is, a standard, in order to establish the probe shape; this is commonly known as probe characterization. Commonly used characterization standards include high precision silicon gratings [3], [7], blades, other AFM tips, colloidal gold articles [12], latex particles [13], etc..

The problems associated with probe characterization are the following. (1) The shape of the characterization standard in never perfectly known and manufacturing tolerances for commercially available standards range from 5 to 20nm [14], which is on the same order of magnitude of the size of the probes themselves [15]. Therefore, the shape of the probe cannot be recovered with the necessary precision. (2) Since probes wear with use, frequent characterizations are necessary to re-establish the probe shape, decreasing inspection throughput and, finally, (3) the standard itself must be kept intact and clean throughout its life span, which adds to process complexity. Therefore, probe characterization has only been used on a qualitative basis, as a means to assess probe wear or detect probe failure.

C. Blind Reconstruction

Another currently used methodology for image deconvolution is the so called blind reconstruction [16], [17], [18] procedure and its variations. This technique allows for estimation of the probe shape without a priori knowledge of the surface of the characterization standard; it, therefore, removes the requirement for any calibration of the standard. However, this estimate consists of only an upper bound for the probe shape and its quality is a strong function of the surface features found on the standard.

Blind reconstruction has its basis on the dilation interpretation for image formation. It assumes, therefore, that the image is essentially the surface of the combined volumes of all translates of the reflected probe tip as the reflected probe apex is lined up with each sample surface point. Thus, the (reflected) probe profile is always bounded by the image. Crude estimates of the probe profile can then be made simply by taking the sharpest features present in the image. That should serve as an upper bound for the AFM probe shape. In fact, if the surface portrays an infinitely sharp protrusion, the image of that surface should be identical to the reflected probe shape, according to Case 4 in section II. For an AFM probe with a single tip (discarding pathological cases of probes with split tips), the blind reconstruction procedure can be reduced to the following recipe: (1) identify peaks in the image, (2) use the peak regions to estimate the reflected probe shape and (3) overlay these estimates, lining up at the peaks and take the minimum envelope of the combined profiles as the reflected probe estimate. Figure 4 illustrates the process.

As mentioned before, since probe estimation by blind reconstruction is implemented using only the image data, the quality of the probe estimate is highly dependent on the image itself, as demonstrated in Ref. [9]. For instance, a smooth surface would yield few distinct peaks in its image and thus have limited utility in this mode of probe estimation. On the other hand, a surface with high aspect ratio features would produce an image with sharp features and therefore a more accurate probe estimate. In Figure 5, we see the resulting probe estimate made using two surfaces with the same peak to peak RMS but with differing correlation lengths (which is the average wavelength of the surface). Clearly, the quality of the probe estimation is significantly better for the surface with the smaller correlation length, that is, with sharper features.

Since it is hard to guess the sharpness of features on the characterization standard, the quality of the estimate cannot be precisely determined either. Therefore, the deconvolved AFM images that use such probe estimates may lack accuracy due to poor probe estimation. This ambiguity in probe estimation can be illustrated as depicted in Figure 6. In short, a certain image can be generated by an infinite number of appropriate sample/probe pairs that satisfy Equation (4).

As a conclusion, even though estimation schemes exist, they still necessitate special characterization standards that have features much smaller than the probe. Such standards maybe difficult to obtain, maintain or characterize. Additionally, for the same reasons laid out in section III-B, frequent estimation may lead to lower throughput. It would be desirable, then, to develop a methodology that does not require special characterization standards, that can deliver high quality probe estimates for image deconvolution, and that does not reduce throughput or increase complexity significantly.

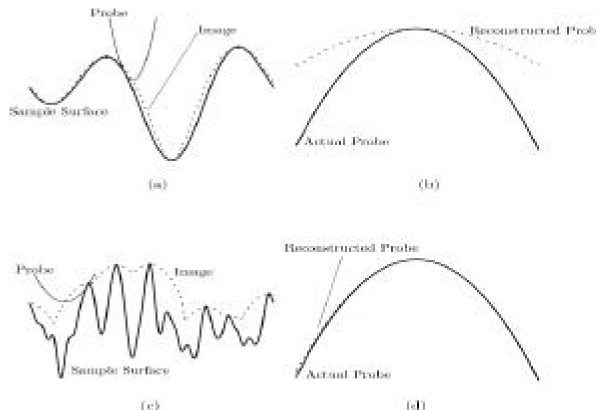

Fig. 5. Probe estimates (individual). (a) Sample surface with large correlation length. (b) Resulting probe estimate is poor. (c) Sample with small correlation length. (d) Resulting probe estimate is good.

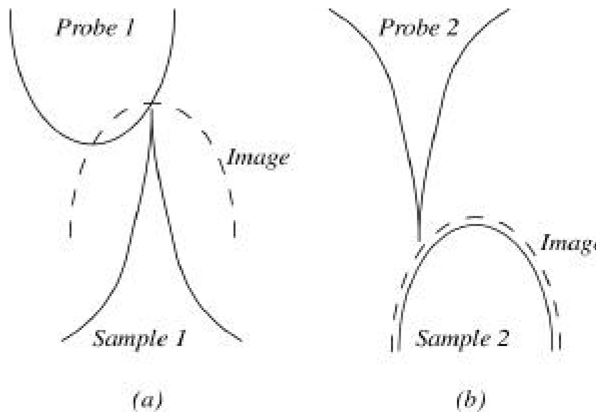

Fig. 6. In both (a) and (b), the same image could be obtained with a swapped set of probe and sample. That is, in both cases, Equation (4) is satisfied. Therefore, the best possible probe estimate (upper bound) is Probe 1 as shown in (a) even though the real probe geometry may be Probe 2 as shown in (b).

IV. STEREO IMAGING

We propose a new approach to image deconvolution called Stereo Imaging. In this approach, two images of the same sample are obtained at different vantage points. That is, the sample is mechanically rotated relatively to the probe prior to the second scan. Since the rotation angle can be specified, one obtains the following system of equations:

$$\begin{aligned} I_1 &= S \oplus P \\ I_2 &= S^* \oplus P \\ S^* &= Rot(S; \theta) \end{aligned} \quad (5)$$

If S is the set of all points $\{x; y\}$ pertaining to the surface of the sample, then S^* will be composed of points $\{x_r; y_r\}$ as determined by the rotation operator shown in Equation (6).

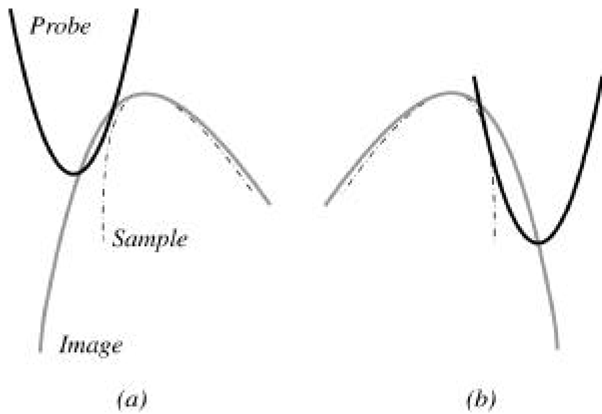

Fig. 7. Two images from different vantage points. (a) Sample tilted by $-\pi/10$ radians and resulting image obtained with the portrayed probe. (b) Second image obtained by rotating the sample by $\pi/10$ radians from the vertical direction. Both images are blunt and distorted versions of the high aspect ratio sample due to convolution.

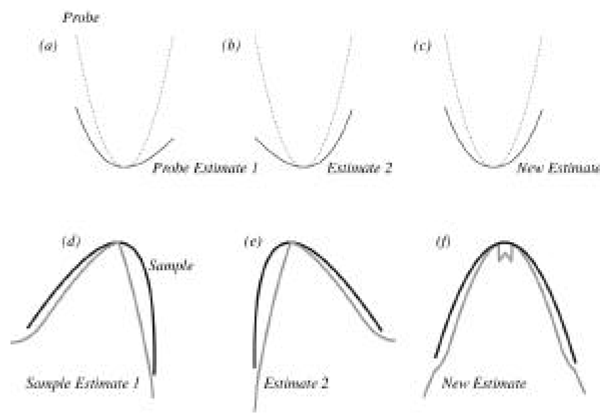

Fig. 8. Probe and sample initial estimation. (a) and (b) portray the results of probe estimation by blind deconvolution for each image. The estimates are significant different than the original probe shape. In (c), estimate combination yields a slightly tighter estimate. (d) and (e) are sample estimations for each vantage point obtained by erosion with the new combined probe estimate. (f) shows the new sample estimate by overlay of the previous estimates. This estimate is somehow closer to the real sample shape but far from precise.

$$\begin{bmatrix} x_r \\ y_r \end{bmatrix} = \begin{bmatrix} \cos(\theta) & -\sin(\theta) \\ \sin(\theta) & \cos(\theta) \end{bmatrix} \begin{bmatrix} x \\ y \end{bmatrix} \qquad (6)$$

Equation (5) defines a system with two equations and two unknowns and therefore can be solved for both probe and sample geometry without the need for prior characterization. The rotation of the sample provides an extra constraint for estimation; as a result, estimation ambiguity is greatly reduced.

The steps involved in stereo imaging include: (1) obtaining two images of the sample; (2) estimating the probe shape by blind deconvolution; (3) combining probe estimates by overlay; (4) generating sample estimates by Erosion; (5) combining sample estimates by overlay; (6) sharpening the probe estimates. Steps (3) though (6) are repeated until convergence is reached. Further explanations follow.

The first step of the methodology consists of obtaining two images of the same sample at different angles as seen in Figure 7. The sample rotation is obtained by means of a high precision tilt actuation system. In this example, the sample is chosen to have a high aspect ratio. Notice how the images are blunter and wider versions of the underlying sample due to convolution. Also, in this example, in the first image the sample is tilted by $-\pi/10$ radians and in the second image, the sample is tilted by $\pi/10$ radians.

Next, blind deconvolution is used to estimate the probe geometry for each image. The estimates are combined by simply overlaying them. A sharper estimate for the probe is obtained. This probe estimate is used to generate sample estimates based on each image. The process of sample estimation given a probe estimate is called Erosion and corresponds to the inverse mechanism of image formation. It can be done by simply scanning the under side of the images with the reflected probe estimate and recording the reflected probe apex position at each translate. Complete discussions on Erosion can be found in Refs. [10], [16], [17] and [18].

The sample estimates are combined to generate a new one by simply overlaying them. Prior to overlay, the sample estimates are brought to an upright position. In Figure 8(f), the notch at the top of new estimate is due to the overlay of the sample estimates. It should be clear at this stage that the overlaying operation relies on an accurate knowledge of the rotation angle θ. Also, if there is any spurious translation during the tilting process, images will be displaced and so will be the initial sample estimates. As a result, during the overlay, sample estimates will fall out of place generating an inaccurate new estimate. This creates the need for high precision tilt actuators (low radial runout). In addition, it requires that the relative position of the rotation axis with respect to the AFM frame be known at all times, which can be achieved by calibration. An alternative to that is the scanning of reference features before and after rotation to allow for identification of any spurious translation that might have occured during tilt.

Now, the new probe estimate must be sharpened in order to satisfy Equation set (5). The process of sharpening the probe estimate includes the following steps: (1) Place probe estimate in a certain point P_1 along the image. (2) Verify if the probe estimate interferes with the sample estimate. (3) Trim or sharpen interfering regions of the probe. (4) Repeat procedure for all points P_i along one image. (5) Repeat procedure for the second image.

The sharpening procedure makes sure that each image is a dilation of the estimated sample by a structuring element with the shape of the reflected probe estimate. That is, it forces the estimates to satisfy Equation set (5).

The sharpening operation reduces ambiguity around sample and probe estimation. This is so because the space of solutions for probe and sample geometry satisfying one constraint as established in Equation (4) is necessarily

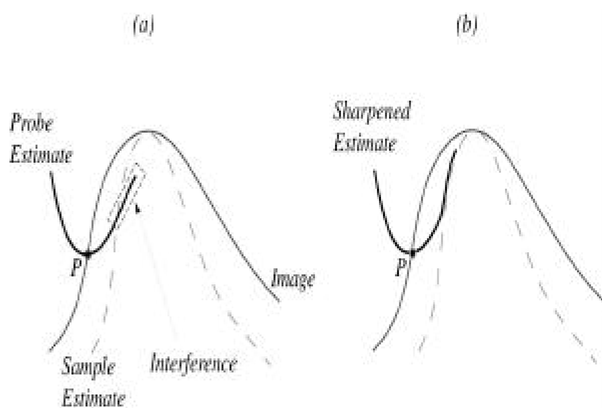

Fig. 9. (a) Probe Estimate must be always externally tangent to sample estimate in order to satisfy Equation (4). Therefore, the interfering region must be trimmed from the probe estimate. As a result, the probe estimate is sharpened as shown in (b).

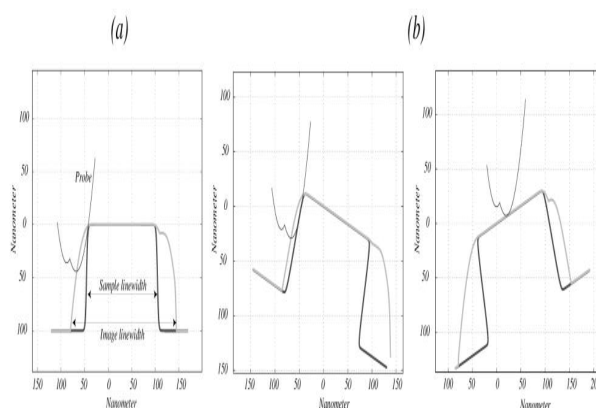

Fig. 11. (a) Conventional AFM image with sample in the upright position (µ = 0). (b) Two images obtained by tilting the sample by µ = §¼=10 radians.

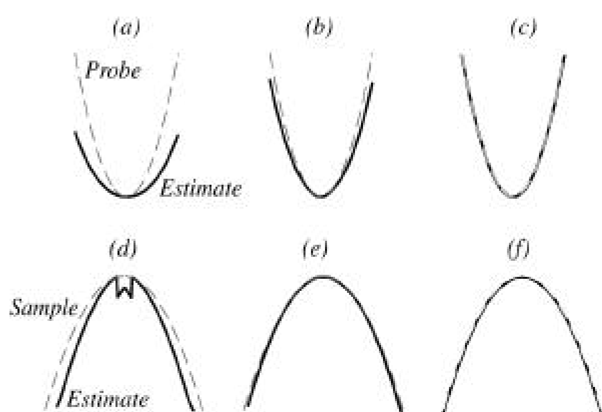

Fig. 10. Evolution of estimates. Sketches (a) and (d) show probe and sample estimates based on a combination of blind estimates. Since the sample is not very sharp, estimates are very inaccurate. Sketches (b) and (e) are the results of the ¯rst iteration of the Stereo Imaging procedure. Estimates are greatly enhanced. Sketches (c) and (f) are the results of the second iteration. Estimates and real geometries are identical; convergence is reached and no signi¯cant geometrical changes happen in further iterations.

larger than the space of solutions that satisfy two constraints, simultaneously, as established in Equation set (5). Consequently, increasing the number of constraints (or images at di®erent angles) will eventually reduce the space to a single solution and zero ambiguity. However, multiple imaging is too time consuming and two images seem enough to accomplish high precision estimates in most cases.

The sharpened probe estimates are then combined by overlay again. New sample estimates are generated by erosion and the whole process is repeated until no noticeable change in the estimates is detectable. That is, until the RMS of the di®erence between probe estimates from one iteration to another is su±ciently small. The evolution of probe and sample estimates is shown in the Figure 10.

V. PRELIMINARY RESULTS

Stereo Imaging allows for precise estimation of probe geometries without a priori probe characterization. That is, probe and sample are estimated simultaneously, and estimation quality is independent of the sample characteristics. In addition to that, tilting of the sample allows the probe to reach otherwise inaccessible regions. Such regions are usually called shadow zones.

Figure 11 (a) shows the cross section of a step feature. It also depicts a probe, in this case with two apices, and the corresponding simulated image. The image is a dilated version of the sample and metrology data obtained from this image would render inaccurate results (image linewidth ¼ 225 nm, sample linewidth ¼ 150 nm). In addition to that, the side walls of the step are never really touched by the probe; therefore, no information about this shadow zone is stored in the image. In this simulation, the step has dimensions compatible with micro features regularly present in semiconductor devices. The probe was chosen to have a complicated geometry with a primary radius of curvature of around 10 nm and a secondary apex. Figure 11 (b) shows two images obtained by tilting the sample. The side walls are now exposed to probe.

The results of both blind deconvolution estimation (obtained from the image depicted in Figure 11 (a)) and stereo imaging estimation (obtained from the images depicted in Figure 11 (b)) are shown in Figure 12. Since the sample has no sharp features, blind estimation provides very poor results. In fact, the probe could not be estimated at all because there were no sharp peaks in the image and, as a result, sample estimation is poor. On the other hand, stereo imaging estimation results are virtually indistinguishable from the original geometries (estimated linewidth ¼ 160 nm). The areas of the estimation close to the base that signi¯cantly di®er from the original sample are actually uncertain reconstruction zones and are °agged by the algorithm, and should be ignored. Uncertain zones happen when the probe estimate is in contact with the sample es-

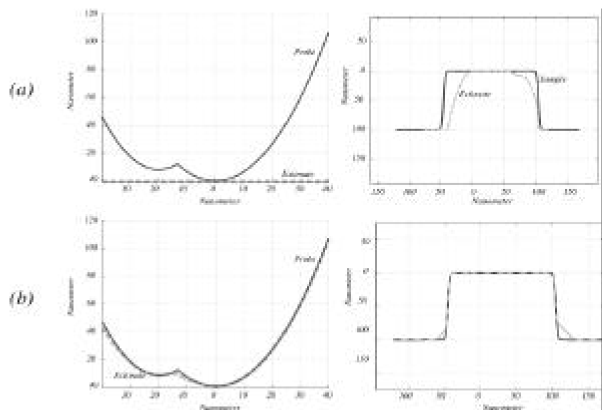

Fig. 12. (a) Probe and sample estimation based on blind deconvolution (State of the Art). (b) Probe and sample estimation based on stereo imaging. Results after 3 iterations.

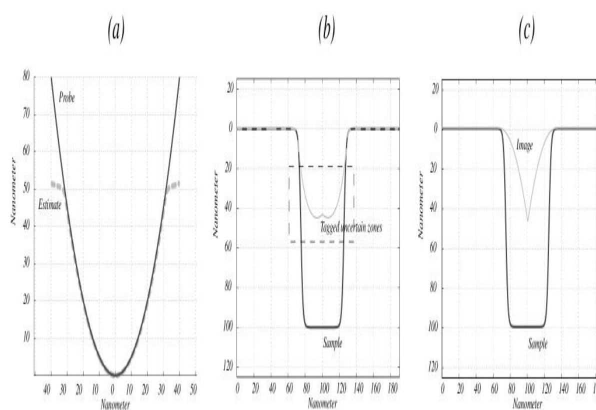

Fig. 14. (a) Probe estimation by stereo imaging. (b) Sample estimation by stereo imaging. Sample rotated $\theta = \pm\pi/20$ radians. Probe with tip radius of $\approx$ 10nm. Results after 5 iterations. (c) Image of the sample with the same probe in upright position.

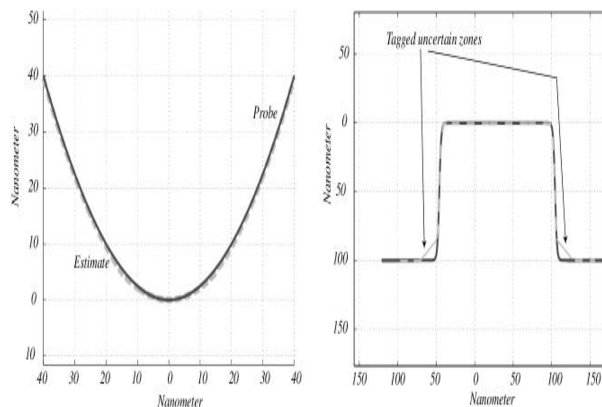

Fig. 13. Probe and sample estimation by stereo imaging. Sample rotated $\theta = \pm\pi/5$ radians. Probe with tip radius of $\approx$ 20nm. Results after 3 iterations.

timate in more than one point simultaneously [8], for a certain position along the image. During scanning, such regions are not touched by the AFM probe, and may be of any depth.

Similar results can be obtained if a probe of completely different geometry is used, as shown in Figure 13. Also notice that the probe geometry used in the simulations is not sharp or slender, compared to the sample geometry. Deconvolution is achieved in spite of probe size or shape. This insensitivity to probe shape and size opens the possibility for using large probes. Such probes maybe coated with Diamond for extended life and maybe utilized for surface strength measurements by micro-indentation, simultaneously with topography measurements.

One limitation of the stereo methodology is that it does not solve the problem of narrow trenches that are inaccessible to the probe. Only high aspect ratio probes at low scan rates, operated in intermittent contact, can access areas deep into the negative steps. However, as seen in Figure 14, the reconstruction obtained with the stereo approach renders good pitch measurement and is a better depiction of the underlying sample than an image of the same sample taken in the usual upright position. The bottom of the trench estimation (solid gray line, Figure 14(b)) is an uncertain reconstruction zone that is automatically tagged by the algorithm. In that zone, the reconstruction sets un upper bound for the sample topography, that is, in that region the real sample may have any depth as long as it is deeper than the boundary set by the estimation.

VI. CONCLUSIONS

Convolution effects may severely distort metrology data obtained with Atomic Force Microscopes. Although some techniques exist that allow for image deconvolution, they mostly fail to deliver high fidelity topography estimates and are cumbersome and time consuming, thus reducing inspection throughput.

By obtaining two or more images of the sample at different vantage points, stereo imaging can be used to generate high precision estimates of both probe and sample simultaneously. Therefore, metrology accuracy is ensured, regardless of probe shape or size. Since the probe geometry is estimated at every imaging event, an effective probe monitoring scheme can be implemented.

Since all steps involved in the Stereo Imaging approach are carried out by set or morphological operations, its generalization to 3-D and volume analysis (instead of the cross-sectional analysis discussed in this paper) is simple.

Finally, the next step of this research project is underway and includes experimental tests with calibrated samples aiming at assessing the repeatability of the method as well as the influence of noise and scan dynamics effects on the final reconstruction results.

References

[1] Semiconductor Industry Association, "International Technology Roadmap for Semiconductors: 2000 update," International SEMATECH, Austin, TX, 2000.

[2] Binning, G., C. F. Quate and Ch. Gerber, "Atomic force microscope," Physical Review Letters 56, pp. 930–933, 1986.
[3] B. D. Aumond and K. Youcef-Toumi, "Experimental High Precision Profilometry of High Aspect Ratio Samples," Proceedings IEEE Int. Conf. on Systems, Man and Cybernetics, San Diego, California, pp. 4435-4440, 1998.
[4] G. S. Pingali and R. Jain, "Restoration of scanning probe microscope images," Proc. IEEE Workshop on Applications of Computer Vision, pp. 282-289, 1992.
[5] B. D. Aumond and K. Youcef-Toumi, "High Precision Stereo Profilometry based on Atomic Force Microscopy Technology," Proceedings of the Mechatronics 2000 Conference, Atlanta, Georgia, September, 2000.
[6] Griffith, J. E. and D. A. Griggs, "Dimensional metrology with scanning probe microscopes," Journal of Applied Physics 74, pp. 83–109, 1993.
[7] D. Keller, "Reconstruction of stm and afm images distorted by finite-size tips," Surface Science 253, pp. 353–364, 1991.
[8] Villarubia, J. S., "Morphological estimation of tip geometry for scanned probe microscopy," Surface Science 321, pp. 287–300, 1994.
[9] Yeo, Y., B. D. Aumond and K. Youcef-Toumi, "Precision atomic force microscope imaging," Proceedings of the IEEE 2000 International Conference on Signal Processing, Beijing, China, 2000.
[10] Yeo, Yee, "Image Processing for Precision Atomic Force Microscopy," Mechanical Engineering M.S. Thesis, MIT, Cambridge, Massachusetts, 2000.
[11] H. Dai, J. H. Hafner, A. G. Rinzler, D. T. Colbert and R. E. Smalley, "Nanotubes as Nanoprobes in Scanning Probe Microscopy", Nature 384, pp. 147-151, 1996.
[12] S. Xu and M. F. Arnsdorf, "Calibration of the scanning (atomic) force microscope with gold particles," J. Microscopy, 173, pp. 199-204, 1994.
[13] Y. Li and S. M. Lindsay, "Polystyrene latex particles as a size calibration for the atomic force microscope," Rev. Sci. Instrum. 62 (11), pp. 2630-2633, 1991.
[14] NT-MDT Co., Commercial standard gratings, AFM equipment and accessories. Block B, South Industrial zone, State Research Institute of Physical Problems, Zelenograd, Moscow, 103460, RUSSIA.
[15] Digital Instruments / Veeco Metrology Group, AFM equipment and accessories. 112 Robin Hill Road, Santa Barbara, California, 93117.
[16] J. S. Villarubia, "Scanned probe microscope tip characterization without calibrated tip characterizers", J. Vac. Sci. Technol. B, 14 (2), 1518-1521 (1996).
[17] P. M. Williams, K. M. Shakesheff, M. C. Davies, D. E. Jackson, C. J. Roberts, and S. J. B. Tendler, "Blind reconstruction of scanning probe image data", J. Vac. Sci. Technol. B, 14 (2), 1557-1562 (1996).
[18] S. Dongmo, M. Troyon, P. Vautrot, E. Delain, and N. Bonnet, "Blind restoration method of scanning tunneling and atomic force microscopy images", J. Vac. Sci. Technol. B, 14 (2), 1552-1556 (1996).